Understanding the mechanism of large-scale template elimination during calcination of Mcm-41

S. Palencia-Ruiz, Alexander Sachse, F. Amar, C. Gucuyener, N. Bats, N. Batalha, L. Pinard

Understanding the mechanism of large-scale template elimination during calcination of Mcm-41

S. Palencia-Ruiz [a], A. Sachse [a], F. Amar [a], C. Gucuyener [b], N. Bats [b], N. Batalha [a,*], L. Pinard [a,**]

[a] Institut de Chimie des Milieux et Matériaux de Poitiers (ICM2P), UMR 7285 CNRS, 4 Rue Michel Brunet, Bâtiment B27, CEDEX 9, 86073, Poitiers, France
[b] Johnson Matthey, PO Box 1 Chilton Site Belasis Avenue, Billingham, TS23 1LB, (Sat Nav: TS23 1LH), UK

ARTICLE INFO

Keywords:
MCM-41
Heat transfer
Calcination
CTAB
Scale-up
Template

ABSTRACT

An in-depth study of the thermal detemplation of the MCM-41 was carried out in a designed setup running with a high catalyst loading. Mapping the temperature along the catalyst bed during detemplation provides an understanding of the heat transfer phenomena involved under (an)aerobic conditions. Comparison between the results obtained at low (TG/DTA study) and high sample loadings (fixed-bed reactor) suggest that oxygen presence modifies the detemplation mechanism and high flows increase the local temperature in the bed due to the exothermic nature of hydrocarbon oxidation. Thermal cracking products detected during calcination may be considered a benchmark to deduce the local conditions in the catalyst bed. Despite the differences in detemplation processes, both environments lead to solids with similar structural properties. The use of advanced analytical techniques, such as 2D GC, led to the proposal of a detailed reaction scheme for the detemplation step.

1. Introduction

Microporous and ordered mesoporous materials are predominantly employed as heterogeneous catalysts and for the adsorption and separation of ions and small molecules [1,2]. Current synthetic methodologies for their preparation commonly involve the use of organic molecules, also known as organic structure-directing agents (OSDAs) or surfactants, that address the assembly pathway and ultimately fill the pore space [3,4]. The first post-synthesis treatment generally aims to remove these organic molecules to liberate the porosity. This process yet might affect the structural properties of the materials and hence their performance in adsorption or catalysis [5,6]. Indeed, numerous reports have correlated the dependence of the detemplation treatment with the catalytic/adsorption properties [7,8].

High temperature (up to 723 K) combustion, which is termed calcination, is the process of choice to remove the template. However, this slow and highly energy-demanding approach might entail detrimental effects on the materials themselves, such as: texture deterioration and disordered arrangement of the porous structure [9], - acute loss of framework elements, e.g., dealumination and depopulation of acid sites [10,11], - and thermal expansion incompatibility among components used in systems such as membrane-based separation devices [12–14]. This detrimental effect was explained by He et al. [15] to result from the dramatic decomposition of the organic guest molecules under large increasing temperature rates, leading to an abrupt increase of the inner pressure. Consequently, alternative routes operating under milder conditions are needed to overcome these drawbacks. Several techniques have been proposed for low-temperature and/or faster detemplation, such as plasma-induced oxidation [16–19], liquid extraction [20], supercritical fluid extraction [21], sonication [22], free-radical mediated oxidation via hydrogen peroxide degradation [23–25], microwave-assisted Fenton-like oxidation [26] and ozonication [27,28]. However, none of these allowed to reach a high technology readiness level and hence still require significant development. In the case of the plasma treatment, the residue from plasma decomposition may remain in the sample because of the low-temperature process and, e.g., induces hydration [29]. In the case of solvent extraction, Jones et al. [30] displayed some limitations of the approach when the OSDA strongly interacts with the framework and when pore openings of the zeolite are smaller than the size of the template molecule. Hence, calcination still

* Corresponding author.
** Corresponding author.
E-mail addresses: santiago.palencia.ruiz@univ-poitiers.fr (S. Palencia-Ruiz), alexander.sachse@univ-poitiers.fr (A. Sachse), fatmaamrar@gmail.com (F. Amar), Canan.Gucuyener@matthey.com (C. Gucuyener), Nicolas.Bats@matthey.com (N. Bats), nuno.rocha-batalha@ircelyon.univ-lyon1.fr (N. Batalha), ludovic.pinard@

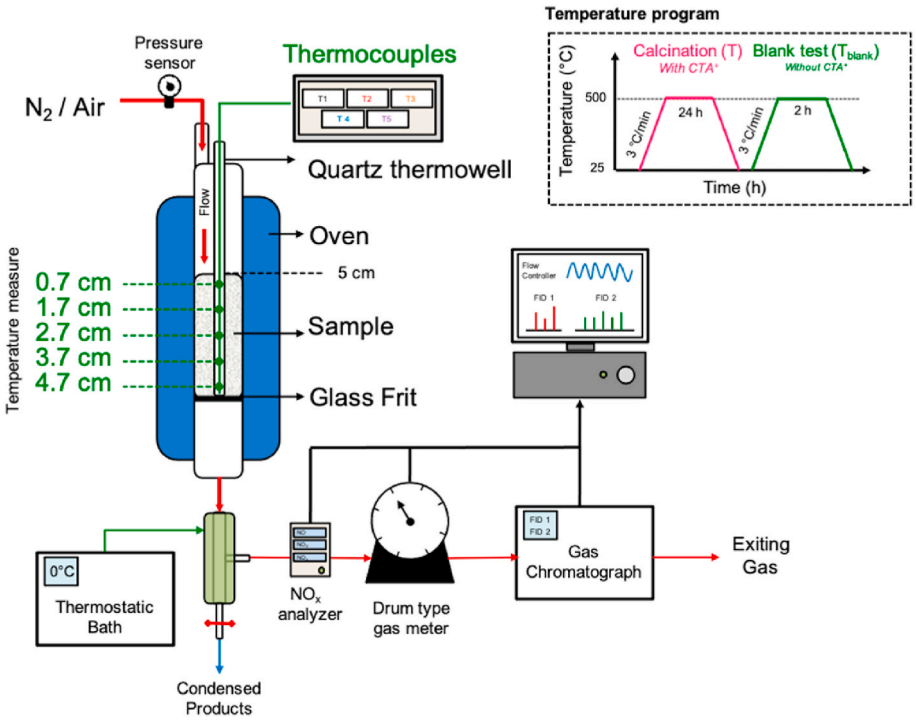

Fig. 1. Experimental setup employed for the thermal detemplation.

seems to be the best solution. Still, a better understanding of heat and mass transfer phenomena is essential to improve this key step, especially developing advanced materials.

While the discussion above clarifies the importance of the calcination approach for achieving and maintaining a high quality of the micro and organized mesoporous materials depending on the application, it totally dismisses the safety risks associated with the effluent composition generated all along the calcination. During calcination, detemplation is achieved not only via oxidation but also by Hoffmann degradation. Under different conditions (temperature, heating rate, atmosphere, mass), each reaction (e.g., oxidation vs. Hoffman degradation) may change as each would have its activation energy and dependence on the template's nature. However, as Hoffman degradation can result in hydrocarbons and amines, the changes in the calcination parameters can easily make the process prone to fire, explosion, and toxic exposure [31].

MCM-41 is a mesoporous material whose pore diameters vary between 2 and 6.5 nm as a function of the chain length of the employed surfactant. In addition, a significant amount of organic material, i.e., 45–55 wt%, is trapped inside the as-synthesized MCM-41, which makes this mesoporous material an ideal candidate for studying in closer detail the template removal phenomena during calcination [32].

Other porous materials, such as zeolites, are commonly synthesized within organic templates but in lower content, e.g., less than 15 wt% in ZSM-5 [31,33]. Moreover, unlike these crystalline microporous, MCM – 41 and other mesoporous solids allow for the recovery of the organic structure-directing components [34]. This is explained by the fact that the individual molecules that form the assembled structure-directing components are held together by weak forces that are easily broken and are sufficiently small to be eliminated through the relatively large mesopores. Furthermore, the interaction energies between the organic (OSDA) and the inorganic (framework) fractions in microporous materials are stronger compared to those from ordered mesoporous materials [35].

Thermogravimetry/differential thermal analysis (TG/DTA) is the primary technique used to understand the mechanism during calcination [7,32,36–44]. Such experiments were carried out in the presence or absence of oxygen but always on a low amount of material (i.e., mg). Hence, hiding the impact in the reaction mechanism as a result of mass and heat transfer limitations that can occur under more industrial conditions, i.e., at high loadings of material. In addition, the analytical devices coupled to TG/DTA are generally mass spectrometry (MS) [36] or gas chromatography [43], which allow the detection and quantification of CO_2, CO, H_2O, and light hydrocarbons, but never of heavy molecules and traces of oxidation products. The small amount of material employed in TG/DTA hinders this trace analysis, making it difficult to establish a detailed detemplation mechanism.

The aim of this study is the calcination of MCM-41 synthesized from hexadecyltrimethylammonium bromide (CTAB) as a surfactant. Calcination is performed with and without oxygen, on a high sample loading (1000 higher than open literature), in an instrumented experimental rig to obtain relevant information on the heat and mass transfer phenomena along the sample bed. In addition, a thorough analysis of the calcination products using conventional and advanced analytical techniques (one and two-dimensional gas chromatography) allowed us to propose a detailed template removal mechanism.

2. Experimental section

Material synthesis: as-synthesized MCM-41 was prepared by adapting a procedure described in the literature [45] using the quaternary ammonium salt, hexadecyltrimethylammonium bromide, as a template. In a typical synthesis, 5 g of CTAB were dissolved in 450 mL of demineralized water. After 15 min of stirring at 25 °C, 17.5 mL of 2 M NaOH solution were added, and the solution was mixed for 30 min. Subsequent heating of the solution was carried out using an oil bath previously heated at 80 °C. 25 mL of tetraethyl orthosilicate (TEOS) were immediately added and left stirring for 2 h. The product was separated by centrifugation and washed with distilled water until reaching a pH of 7. The as-synthesized solid was finally dried at 80 °C for12 h.

Materials characterization: The X-ray diffraction (XRD) patterns were obtained on an Empyrean PAN analytical with Cu-Kα emission ($\lambda = 1.54$ Å) in the range 2θ of 0.5–7°. Nitrogen physisorption isotherms at −196 °C were measured on a Micromeritics TRIFLEX instrument. The specific surface area was determined using BET. Before measurements,

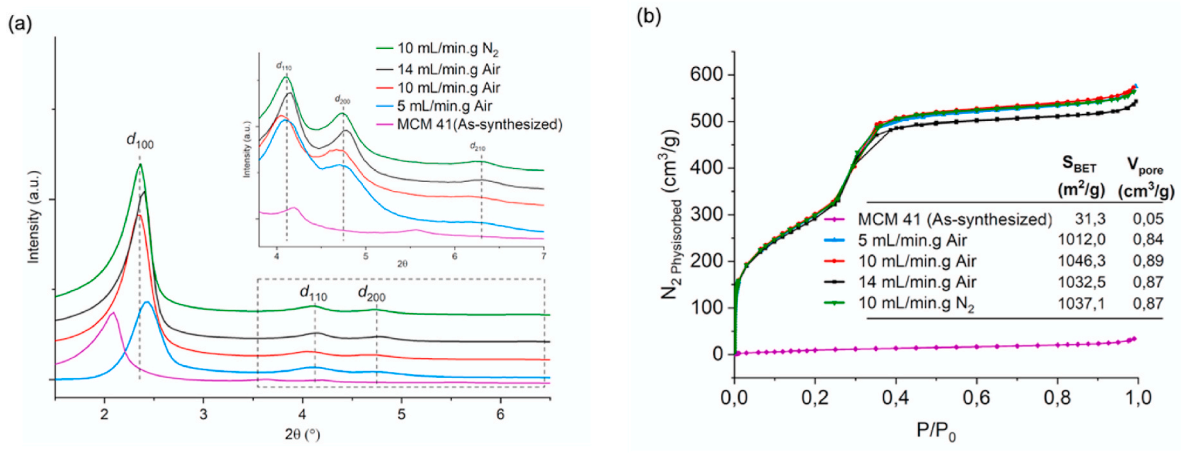

Fig. 2. X-ray diffractograms (a) and N_2 physisorption isotherms at −196 °C (b) of MCM-41 before and after calcination under air and N_2 atmosphere.

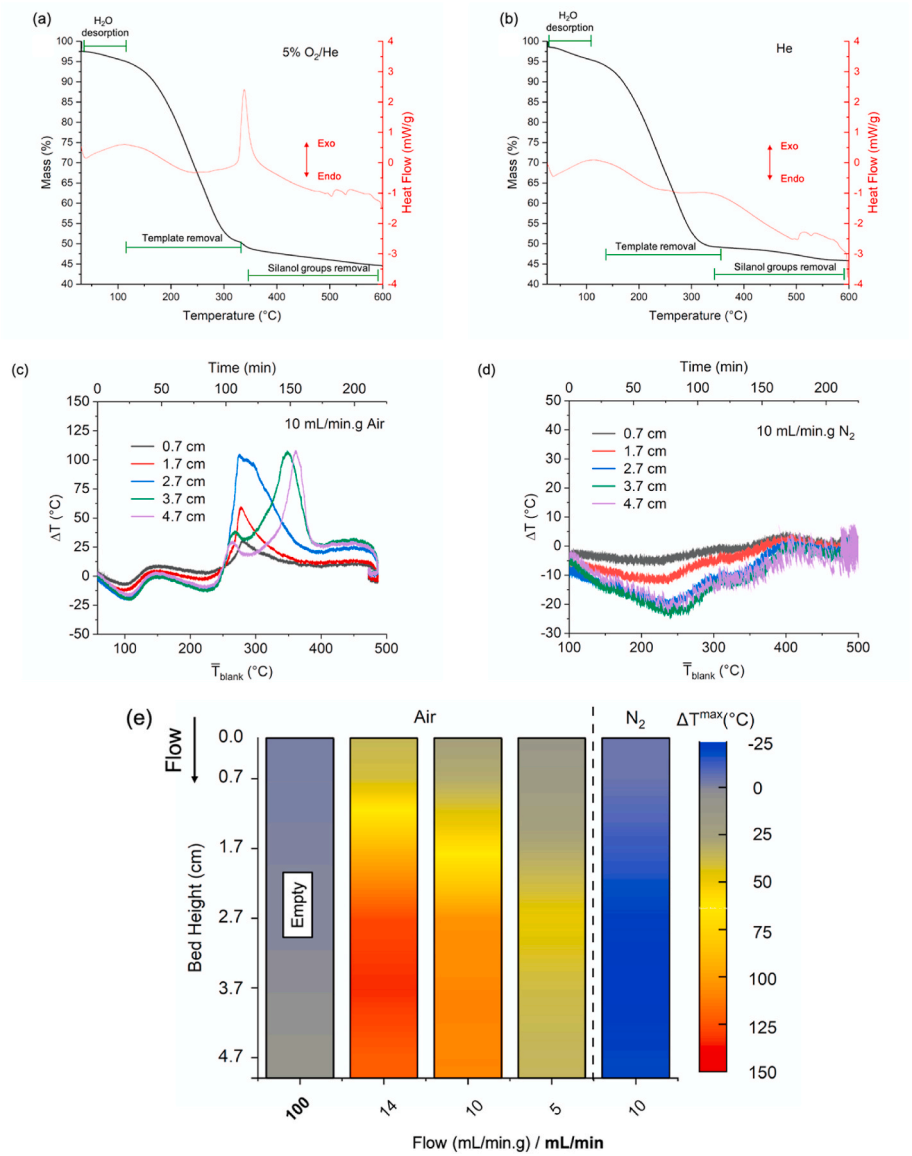

Fig. 3. TG/DTA analysis of MCM-41 under 5%O_2/He (a) and pure He (b) ΔT (the difference between the temperatures on the sample with and without the template) as a function of $\overline{T}_{blank}$ (the average temperature of the sample bed without CTA^+), at different heights on the sample bed, under a flow of 10 mL/min.g in air (c) and N_2 (d). Maximal temperature variation peaks (ΔT^{max}) along the sample bed under different operating conditions (e).

the samples were exposed to a secondary vacuum at 25 °C for 1 h to avoid removing organic traces from the organized mesoporous material [46]. Elemental analysis of the organic (CNH) and inorganic (Br) were performed on a Thermo Flash 2000 analyzer and ED-XRF EPSILON 4 (PANALYTICAL) equipped with a tube containing an anode of Ag (15W–50 kV – 3 mA), respectively.

Thermal detemplation followed by thermogravimetry/differential thermal analysis: TG/DTA was carried out on an SDT Q600 TA instrument under aerobic (5% O_2/He) and anaerobic (He) flows. 7 mg of the solid were introduced in a crucible, then heated from 25 °C to 500 °C with a temperature ramp of 10 °C/min under a gas flow of 100 mL/min.

The thermal detemplation in a fixed-bed reactor (Fig. 1): The calcination of the as-synthesized MCM-41 was carried out under atmospheric pressure in a top-flow-fixed-bed reactor. 7 g of sample, previously sieved between 0.2 and 0.4 mm, were charged. The height and diameter of the sample bed were 50 and 25 mm, respectively. The air (or nitrogen) flow rate varied from 35 to 100 mL/min. During the calcination, the reactor temperature was increased from 25 to 500 °C with a heating rate of 3 °C/min and maintained for 24 h. Temperature (T) was recorded using five thermocouples (Type K, 10 data/s) located inside a quartz thermowell at different heights in the flow direction, viz. Top: 0.7 and 1.7; Middle: 2.7; Bottom: 3.7, and 4.7 cm. After cooling down the reactor, the calcined solid was heated again using the same protocol to obtain the thermal profile of the sample without a template (T_{blank}, Fig. 1). Three parameters were set:

- $\Delta T = T - T_{blank}$: the difference between the temperatures recorded on the sample with and without template (CTA^+). It is worth mentioning that this parameter is proportional to a heat flow ($Q = \dot{m} \cdot C_P \cdot \Delta T$, where Q is the flow rate and C_p is the specific heat capacity at constant pressure) (SI, Fig. S1).
- ΔT^{max}: the maximal difference in temperature recorded at each point of the sample bed.
- $\overline{T}_{blank}$: the average temperature of the sample bed without CTA^+.

The exhaust gas was sent through a condenser set at 10 °C. Aqueous and organic phases (named "H_2O & polar components" and "apolar components", respectively), were recovered, separated, and weighted. The organic phase was analyzed outline by GC/FID (Scion 456) and comprehensive GCxGC-MS analyses. GCxGC-MS analysis was performed in a modified Agilent 6890 N gas chromatograph equipped with a two-stage thermal modulator (Zoex Corporation, Houston, TX). A modulation period of 12 s was used. The secondary column effluents were analyzed using a mass selective detector Agilent 5975B, with an acquisition of 22 scans per second in the mass range of 45–300, which corresponds to 7 data points per peak and peak width of 1530 ms. Two capillary columns performed the separation by, the first is a moderately polar VF1701 column (30 m × 0.25 mm × 0.25 μm), and the second column is an apolar DB1 column (2 m × 0.1 mm × 0.1 μm). The first oven was heated at 50 °C for 5 min, then went to 300 °C within a temperature ramp of 1.8 °C/min. The second oven temperature started at 50 °C and immediately heated to 320 °C (1.8 °C/min). NIST-MS 2011 database was used for peak identification.

The non-condensed phase was analyzed online by gas chromatography equipped with two columns (BR899859-105 BRUKER; 30 m × 0.32 mm x 5 μm and SA 0355 AGILENT (1.0 m × 3.18 mm x 2.0 mm), a methanizer coupled to a flame ionization detector (FID). The frequency of GC analyses was about 5 min. In addition, NO_x products were monitored using an AC32 M ENVIRONNEMENT SA analyzer.

A pressure sensor measures the potential pressure drop (which remained below 0.5 bar), and a drum-type gas meter records the output gas flow.

The calculation of the product yield is described in the supplementary information (SI, section S1).

Thermal detemplation followed by FTIR: Operando detemplation was carried out on an IR cell coupled to a Fourier Transform Infrared (FTIR) spectroscopy (NEXUS NICOLET 5700 spectrometer, resolution of 2 cm^{-1}). As-synthesized MCM-41 was pressed into a thin 2 cm^2 wafer of 10 mg and calcined in the IR cell under air or N_2 flow (100 mL/min) from 200 to 500 °C with an increment of 50 °C. Spectra were acquired after 10 min at each temperature.

3. Results and discussion

3.1. Characterization of the as-synthesized material

XRD pattern of the as-synthesized MCM-41 in Fig. 2 a displays three peaks and one barely observable peak in the low angles range (1–7° 2θ), which can be indexed to the (001), (110) and (200) and (210) reflections, respectively, characteristics of MCM-41 [38,47]. The N_2 physisorption isotherm in Fig. 2 b presents no nitrogen uptake indicating negligible microporosity and mesoporosity. The CTA^+ template is occluded in the pores, thus hindering any possible gas diffusion/adsorption inside the structure. Elemental analysis of the as-synthesized sample displays a C/N atomic ratio of 19/1, confirming that CTA^+ is present inside the structure. Furthermore, only traces of bromine are present (>0.03 wt %).

3.2. Thermal detemplation followed by TG/DTA analysis

The thermogravimetric and differential thermal analysis curves of as-synthesized MCM-41 under air and nitrogen are shown in Fig. 3a and b, respectively. Under aerobic conditions, oxygen flow supplied is stoichiometrically in excess to completely oxidize the occluded template (O_2:CTA^+ molar ratio of 111:1 after reaching 500 °C). Nevertheless, independent of the nature of the gas, the weight loss is similar, ca 55 wt %, suggesting that complete CTA^+ removal is possible even under an inert atmosphere. At 120 °C, a weight loss of ca. 5 wt% and a negative heat flow are attributed to water desorption. Subsequent mass loss of 43 wt% is achieved between ~150 and 400 °C and assigned to the thermal decomposition of the surfactant. According to differential thermal analysis, two reactions appear under air: endothermic reactions followed by exothermic reactions after heating at 320 °C (probably combustion), whereas only endothermic reactions occur under nitrogen. Finally, from 400 °C, whatever the atmosphere, the mass loss (ca 7 wt%) is attributed to the condensation of silanol groups [48].

3.3. Heat and mass transfer in a fixed-bed reactor during detemplation

The calcination of as-synthesized MCM-41 is investigated under industrially more relevant conditions, i.e., a fixed-bed reactor (Fig. 1). Fig. 3c and d compare ΔT as a function of $\overline{T}$ blank, at different heights on the sample bed, with and without oxygen, respectively. ΔT is the temperature difference of samples with and without template and $\overline{T}$ blank is the average temperature of the sample bed without CTA^+. 14 and 5 mL/min.g airflow results can be found in Fig. S2a and b.

Only endothermic reactions occur under an inert atmosphere ($\Delta T < 0$ °C). The negative gradient increases in the flow direction but remains limited (>−20 °C). Inlet oxygen flow is significantly below the stoichiometric amount necessary to completely oxidize all the surfactant occluded (O_2:CTA^+ molar ratio of 4:1 after reaching 500 °C under 14 mL/min.g). Yet, in an aerobic environment, as observed by TG/DTA, three successive reactions take place: desorption of water at 120 °C, then endothermic reactions, followed by exothermic reactions. Furthermore, the measured ΔT, which can be assimilated to a heat flow, shifts, and increases from the top to the bottom of the sample bed, suggesting a significant heat transfer. The ΔT can be higher than 130 °C than the input temperature. At the top of the bed, a narrow thermal gradient peak is observed at $\overline{T}$ blank = 300 °C. This exothermic peak can be correlated with partial oxidation of the evolved surfactant (e.g., oxidation toward

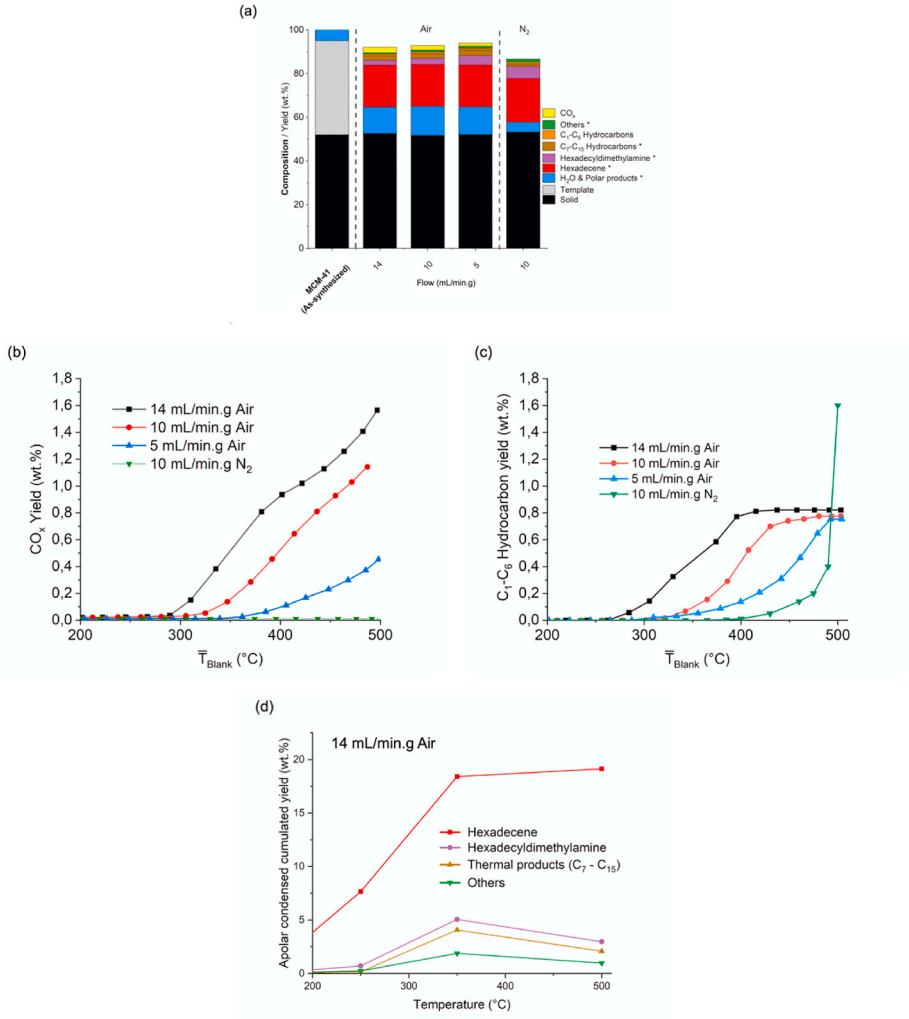

Fig. 4. Products yield under different flows of air and N_2. (a). The yield of (CO_x) CO and CO_2 (b) and C_1–C_6 hydrocarbons (c) as a function of the average temperature of the sample bed without CTA^+. Cumulative: condensed products yield as a function of the input temperature under 14 mL/min.g Air (d).

ketones, cf. GC x GC results). At the middle of the sample bed, this exothermic peak is broader, which may result from the heat released from partial and complete oxidation, allowing it to reach the local temperature leading to the ignition of the template. Subsequently, after removing almost all the surfactant molecules, extinction of the combustion is observed. At the bottom, the first thermal gradient is present but less intense, suggesting a lack of oxygen. However, a more important thermal gradient appears and cannot be correlated to the template oxidation but from the heat released upstream. Consequently, the shift between these two peaks is higher at lower flows because the heat issue of the exothermic reactions is transferred through an insulator material (SI, Fig. S2 a and b). The thermal profile is shown in Fig. 3e through a color shade of the ΔT at different positions on the sample bed. The absence of a thermal gradient with the empty reactor indicates that the sample bed is in the isothermal zone of the furnace. Under nitrogen, the thermal gradient is relatively homogeneous, while in air, it is significant and depends on the gas flow rate. The higher the gas flow rate, the higher the thermal gradient along the sample bed, which is indicative of the role of the gas phase in the dissipation of the heat. Under airflow, thermal phenomena may be described by following the sequence: heat released from partial and complete oxidation → Ignition → Extinction → Heat transfer.

The different behavior between endothermic and exothermic processes observed with and without oxygen may impact the detemplation efficiency. Yet, independent of the inlet gas, all the organic compounds are removed (SI, Table S1), suggesting that oxygen is not indispensable for the CTA^+ removal. Mesopore volume, BET surface area, and the shape of the nitrogen isotherms are similar even under an anaerobic medium (Fig. 2b). Besides, the XRD patterns of the "detemplated" (calcined) solids are similar and display a well-ordered structure formed from hexagonal arrays (Fig. 2a) [38,47]. Peaks slightly shift toward higher 2theta values after treatment (2.4–2.6° 2θ), which correlates to d-*spacing* shrinking because of template removal and silanol groups polycondensation [42,44]. Overall, considering the similar textural properties of the materials obtained after calcination under different environments, treatment under anaerobic conditions could be considered an attractive alternative to preventing thermal runaway issues during calcination [49].

The endo and exothermic reactions involved during the detemplation suggest that a reaction other than combustion is taking place, and therefore the product selectivity might change with the gas nature. The products of detemplation can be divided into four categories: i) combustion products (CO_x, water & polar products), ii) cracking products (C_1–C_6 and C_7–C_{15} hydrocarbons), iii) decomposition products (hexadecene and hexadecyldimethylamine), and iv) trace (named "others"). The bar chart in Fig. 4 a compares the composition of the as-synthetized MCM-41 (drawn from TG) with the weight yield of products under nitrogen and air and different flow rates. It is worth mentioning that independent of the operating conditions; the mass balance ranges between 90 and 98 wt%.

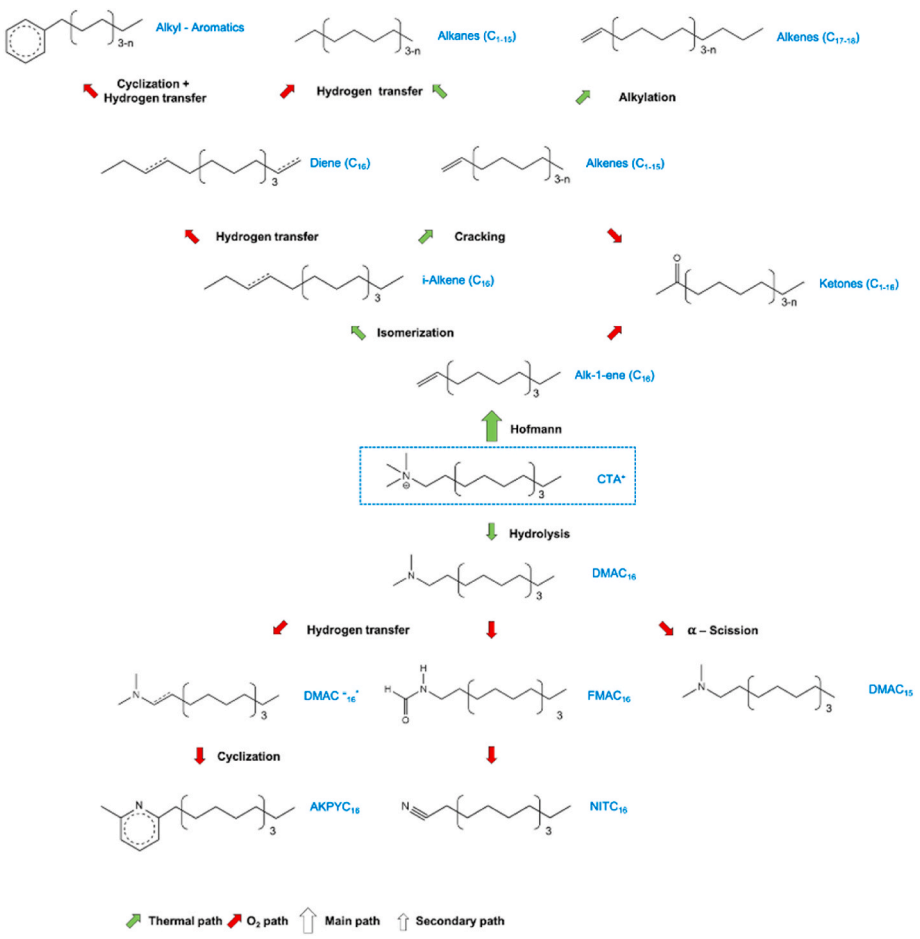

Fig. 5. Reaction scheme of MCM-41 detemplation with and without oxygen. Notation: Hexadecyltrimethylammonium (CTA^+), Hexadecene (Alk-1-ene), Hexadecyldimethylamine ($DMAC_{16}$), Olefin-amines (not-detected*, DMAC $^{=}_{16}$), Alkyl-Pyridines ($AKPYC_{16}$), Hexadecylformamide ($FMAC_{16}$), Hexadecanenitrile ($NITC_{16}$), Pentadecylamine ($DMAC_{15}$).

The quantity of water recovered during the anaerobic treatment is close to the water content obtained from the TG/DTA analysis, respectively 4.5 and 5 wt %. Differently, under aerobic conditions, the quantity of condensed water (and polar products) is higher mainly due to the water produced by the combustion of surfactant and the condensation of silanols due to high-temperature gradients (cf. 3.2 and 3.4). In summary, the higher yields of water and polar products observed in an aerobic environment result from the oxidation reactions.

CO_x products (mainly CO_2) are only detected under airflow, resulting, as expected, from the combustion of the organic surfactant. Regardless of the operating conditions, the CO_x yield remains limited (<2 wt%, Fig. 4a). Therefore, when considering the CO_2 yield, calculating an adiabatic ($T_{adiabatic}$) temperature becomes possible (SI, section S2). Despite the process conditions, the average temperature on the sample bed is close to 15–20 °C of the experimental value, which suggests that the heat losses are limited and that a low CO_2 yield is sufficient to increase the temperature by more than 100 °C. If all the CTA^+ were burned, the heat released would increase the temperature on the sample bed up to 2500 °C (SI, Table S2), which would be extremely harmful to the material and may cause safety issues. Fig. 4b displays the yield into CO_x as a function of the average temperature within the sample bed without CTA^+. The formation of oxidation products shifts towards lower temperatures as the gas flow rate increases. This could mean that the amount of oxygen is insufficient for complete combustion, but as shown previously (Fig. 3e), the higher the gas flow, the higher the thermal gradient on the sample bed. Therefore, the early appearance of CO_x is more likely to be due to an increase in the local temperature than to an oxygen substoichiometry. Indeed, this conclusion is supported by the formation of cracking products at relatively low temperatures, i.e., <300 °C. Thermal cracking (experiment under nitrogen) occurred at temperatures above 400 °C rather than below 300 °C (Fig. 4c).

Hexadec-1-ene is the main detemplation product with a yield of ca. 20 wt%, with and without oxygen; this excludes the Cope elimination mechanism. Indeed, this reaction is an elimination of the *N*-oxide to form alkene and hydroxylamine, thus requiring the prior oxidation of the amine to *N*-oxide. So, the alpha-olefin results from the removal of trimethylamine (TMA) from CTA^+ only through the Hofmann elimination mechanism as proposed by Beck et al. [37]:

$$[CTA^+; SiO^-] \rightarrow \text{Alk-1-ene} + TMA + SiOH.$$

TMA is not condensed owing to the low boiling point, i.e., 3 °C (Temperature of condenser = 10 °C). The Hofmann elimination is an endothermic reaction that begins below 250 °C and is complete at 350 °C (Fig. 4d). Hence, the second negative heat flow observed in this temperature range on TG/DTA can be attributed to the Hofmann elimination. The GC analysis shows that one part of the hexadec-1-ene isomerizes (double bond position), the other part cracks into lighter olefins C_1–C_6 (1 wt%), and C_7–C_{15} (2.5 wt%).

Hexadecyldimethylamine ($DMAC_{16}$) is the second main product (2–6 wt %) and probably results from a hydrolysis mechanism:

$$CTA + + SiO\text{-} + H_2O \rightarrow DMAC_{16} + CH_3OH + SiOH.$$

Its yield is higher without oxygen due to the lower local temperature. Indeed, in the presence of oxygen, formation starts from 250 °C, passes

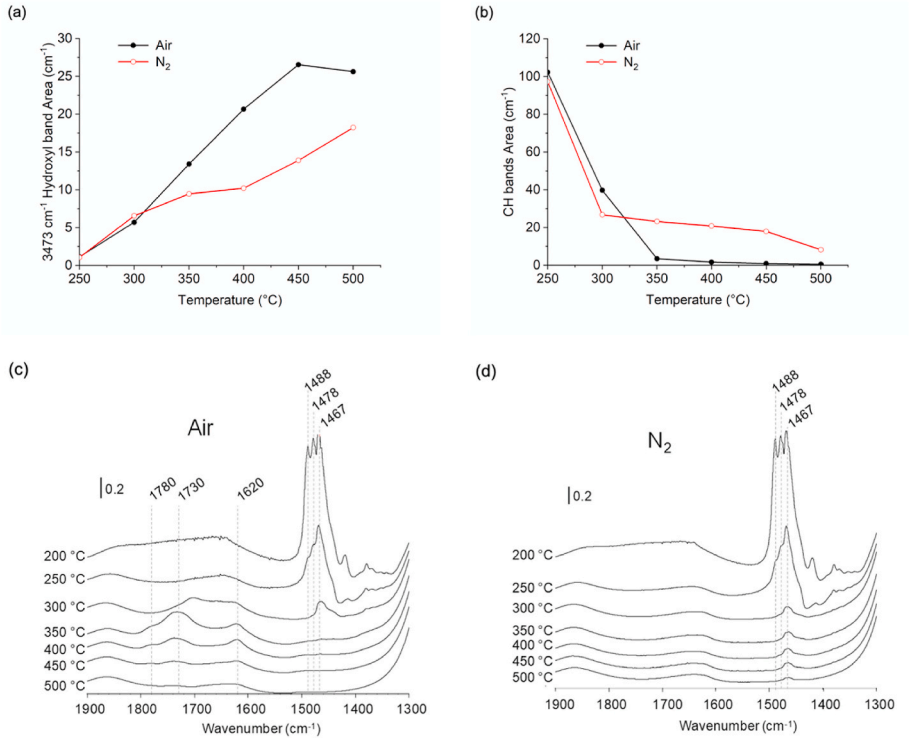

Fig. 6. Evolution of hydroxyl (a) and CH (b) stretching bands as a function of the temperature with and without oxygen. IR spectra, in 1300–1900 cm^{-1} region at different temperatures in the presence (c) and absence (d) of oxygen.

to a maximum at 350 °C, and then decreases (Fig. 4d). The thermal decomposition of $DMAC_{16}$ probably occurs from 350 °C. As local temperatures are higher in the presence of oxygen (Fig. 3e), the yield of $DMAC_{16}$ is lower than in anaerobic media.

Trace composition ("others" and 4th lump) is established by GCxGC/MS analysis (SI, Fig. S3). Surprisingly, octadecene is detected, suggesting that alkylation reactions occur, resulting in hydrocarbon chain growth. The presence of diolefins, alkanes, and aromatics means that hydrogen transfer occurs mainly in the presence of oxygen due to increased local temperature. In addition, some oxidation intermediates such as ketones and hexadecylformamide ($FMAC_{16}$) and hexadecanenitrile ($NITC_{16}$) are detected. Photographic evidence of the liquid samples recovered after calcination through condensation (SI, Fig. S4) displays a clear solution obtained from inert gas treatment compared to the resulting from oxidizing environments, which agrees with the oxidized components detected by GCxGC/MS analysis.

Fig. 5 summarizes the main (Hofmann elimination), secondary (hydrolysis), and side (oxidation, alkylation, isomerization, cyclization, etc.) reactions that occur during detemplation in aerobic (oxygen path) and anaerobic (thermal path) conditions.

Previous studies of the thermal decomposition of the MCM-41 agree that the Hofmann elimination is the main process taking place during calcination. However, it is also suggested that a secondary mechanism may occur. Cope elimination was proposed, but no clear evidence was presented [42]. In this context, our results demonstrate that removal of the template does not require the presence of oxygen, which is required for Cope elimination to take place; yet in both cases, a similar yield of products was obtained.

Investigations of calcination on zeolite *BEA [5] revealed that the detemplation mechanism is, in this case, impacted by acid sites of the framework. Furthermore, in the case of the SAPO-34 study [6], this strong interaction between the acid sites and the template may hinder the complete removal of the OSDA under an inert environment. Hence, the results of the different parameters studied in this investigation, i.e., greater scale and gas environment impact, open a wide window of research that will be addressed over the OSDA employed [44,50,51] and/or micro and organized mesoporous materials type regarding the heat and transfer phenomena taking place inside the calcination bed.

3.4. *Thermal detemplation followed by FTIR*

In order to study the behavior of chemical properties on the surface of the MCM-41 during detemplation, operando experiments with and without oxygen are carried out during heating from 25 to 500 °C. Fig. 6a and b shows the evolution of the area of the silanol band at 3473 cm^{-1} and the sp^3 C–H stretch bands as a function of the input temperature, respectively. The silanol appears from 250 °C regardless of the atmosphere. Indeed, as demonstrated previously, Hofmann elimination occurs below 250 °C (Fig. 4d). The intensity of the silanol band increases rapidly in the presence of oxygen. It passes through a maximum at 450 °C, suggesting a possible increase in the local temperature of the material over the wafer as a result of auto-ignition, which could lead to silanol condensation as inferred from TG/DTA (Fig. 3a and b). The appearance of the silanol band is concomitant with the disappearance of the bands of sp^3 C–H bend (1488 and 1467 cm^{-1}) and N–H bend (1478 cm^{-1}) [39]. In addition, in the presence of oxygen, carbonyl stretching bands appear from 300 °C at 1780 and 1730 cm^{-1}. The lower wavenumber could correspond to saturate aldehyde while the higher to a cyclic ketone. The presence of the carbonyl group indicates that combustion occurs, leading to an increase in local temperatures over the wafer.

4. Conclusion

The results discussed here suggest that the elimination of hexadecyltrimethylammonium occluded in the as-synthetized MCM-41 mesoporous material does not require the presence of oxygen to occur. Indeed, we have successfully shown that template removal can be achieved even under inert gas flow leading to the total elimination of organic species, leading to a similar structural impact. It is worth

recalling that herein, we studied for the first time the calcination of the MCM-41 using higher loads than ever reported in previous studies, which allowed us access to the heat transfer phenomena taking place inside the bed. It was deduced that aerobic environments accelerate the degradation because of heat transfer provided by exothermic oxidation reactions. High air flows increase heat transfer along the calcination bed, which provides the conditions necessary for thermal cracking reactions while heating below 400 °C. The cracking products may be a reliable hint of the actual conditions during the calcination. The removal of occluded hexadecyltrimethylammonium in the as-synthesized MCM-41 occurs primarily by Hofmann elimination and therefore does not require the presence of oxygen. A second mechanism was proposed, based on hydrolysis, in which the major product, hexadecyldimethylamine, is more prone to crack and be oxidized. Detemplation in an inert atmosphere avoids thermal runaway and hence allows the recovery of the long carbon chain alpha-olefin hexadec-1-ene in high purity. The presence of oxygen leads to incomplete combustion and overheating of the catalyst bed, which accelerates the reaction and slightly alters the product selectivity. Hence, exploring different organic templates and oxygen impacts regarding the detemplation mechanism may be interesting. A similar study will be of interest for the calcination of hierarchical zeolites.

[1] F. Akhtar, L. Andersson, S. Ogunwumi, N. Hedin, L. Bergström, Structuring adsorbents and catalysts by processing of porous powders, J. Eur. Ceram. Soc. 34 (2014) 1643–1666, https://doi.org/10.1016/j.jeurceramsoc.2014.01.008.

[2] A. Corma, A. Martínez, V. Martínez-Soria, J.B. Montón, Hydrocracking of vacuum gasoil on the novel mesoporous MCM-41 aluminosilicate catalyst, J. Catal. 153 (1995) 25–31, https://doi.org/10.1006/jcat.1995.1104.

[3] J. Zhang, H. Ding, Y. Zhang, C. Yu, P. Bai, X. Guo, An efficient one-pot strategy for synthesizing hierarchical aluminosilicate zeolites using single structure-directing agent, Chem. Eng. J. 335 (2018) 822–830, https://doi.org/10.1016/j.cej.2017.10.171.

[4] S. Du, X. Chen, Q. Sun, N. Wang, M. Jia, V. Valtchev, J. Yu, A non-chemically selective top-down approach towards the preparation of hierarchical TS-1 zeolites with improved oxidative desulfurization catalytic performance, Chem. Commun. 52 (2016) 3580–3583, https://doi.org/10.1039/c5cc10232d.

[5] E. Bourgeat-Lami, F. Di Renzo, F. Fajula, P.H. Mutin, T. Des Courieres, Mechanism of the thermal decomposition of tetraethylammonium in zeolite .beta, J. Phys. Chem. 96 (1992) 3807–3811, https://doi.org/10.1021/j100188a044.

[6] Q. Qian, D. Mores, J. Kornatowski, B.M. Weckhuysen, Template removal processes within individual micron-sized SAPO-34 crystals: effect of gas atmosphere and crystal size, Microporous Mesoporous Mater. 146 (2011) 28–35, https://doi.org/10.1016/j.micromeso.2011.05.024.

[7] S. Hitz, R. Prins, Influence of template extraction on structure, activity, and stability of MCM-41 catalysts, J. Catal. 168 (1997) 194–206, https://doi.org/10.1006/jcat.1997.1659.

[8] W. Dai, W. Kong, L. Li, G. Wu, N. Guan, N. Li, The effect of organic impurities originating from the incomplete combustion of organic templates on the methanol-to-olefins reaction over SAPO-46, ChemCatChem 2 (2010) 1548–1551, https://doi.org/10.1002/cctc.201000213.

[9] Q. Sun, X. Hu, S. Zheng, Z. Sun, S. Liu, H. Li, Influence of calcination temperature on the structural, adsorption and photocatalytic properties of TiO2 nanoparticles supported on natural zeolite, Powder Technol. 274 (2015) 88–97, https://doi.org/10.1016/j.powtec.2014.12.052.

[10] M.C. Silaghi, C. Chizallet, J. Sauer, P. Raybaud, Dealumination mechanisms of zeolites and extra-framework aluminum confinement, J. Catal. 339 (2016) 242–255, https://doi.org/10.1016/j.jcat.2016.04.021.

[11] W. Lutz, H. Toufar, D. Heidemann, N. Salman, C.H. Rüscher, T.M. Gesing, J. C. Buhl, R. Bertram, Siliceous extra-framework species in dealuminated Y zeolites generated by steaming, Microporous Mesoporous Mater. 104 (2007) 171–178, https://doi.org/10.1016/j.micromeso.2007.01.028.

[12] M. Lassinantti Gualtieri, C. Andersson, F. Jareman, J. Hedlund, A.F. Gualtieri, M. Leoni, C. Meneghini, Crack formation in α-alumina supported MFI zeolite membranes studied by in situ high temperature synchrotron powder diffraction, J. Membr. Sci. 290 (2007) 95–104, https://doi.org/10.1016/j.memsci.2006.12.018.

[13] J. Hedlund, F. Jareman, Texture of MFI films grown from seeds, Curr. Opin. Colloid Interface Sci. 10 (2005) 226–232, https://doi.org/10.1016/j.cocis.2005.09.009.

[14] J.L. Agudelo, E.J.M. Hensen, S.A. Giraldo, L.J. Hoyos, Influence of steam-calcination and acid leaching treatment on the VGO hydrocracking performance of faujasite zeolite, Fuel Process. Technol. 133 (2015) 89–96, https://doi.org/10.1016/j.fuproc.2015.01.011.

[15] J. He, X. Yang, D.G. Evans, X. Duan, New methods to remove organic templates from porous materials, Mater. Chem. Phys. 77 (2003) 270–275, https://doi.org/10.1016/S0254-0584(01)00557-0.

[16] T.L.M. Maesen, H.W. Kouwenhoven, H. Van Bekkum, B. Sulikowski, J. Klinowski, Template removal from molecular sieves by low-temperature plasma calcination, J. Chem. Soc. Faraday Trans. 86 (1990) 3967–3970, https://doi.org/10.1039/FT9908603967.

[17] V. Medvecká, D. Kováčik, A. Zahoranová, M. Stupavská, M. Černák, Atmospheric pressure plasma assisted calcination of organometallic fibers, Mater. Lett. 162 (2016) 79–82, https://doi.org/10.1016/j.matlet.2015.09.109.

[18] S. Bhattacharyya, G. Lelong, M.L. Saboungi, Recent progress in the synthesis and selected applications of MCM-41: a short review, J. Exp. Nanosci. 1 (2006) 375–395, https://doi.org/10.1080/17458080600812757.

[19] Y. Liu, Y. Pan, Z.J. Wang, P. Kuai, C.J. Liu, Facile and fast template removal from mesoporous MCM-41 molecular sieve using dielectric-barrier discharge plasma, Catal. Commun. 11 (2010) 551–554, https://doi.org/10.1016/j.catcom.2009.12.017.

[20] T. Aumond, L. Pinard, C. Batiot-Dupeyrat, A. Sachse, Non-thermal plasma: a fast and efficient template removal approach allowing for new insights to the SBA-15 structure, Microporous Mesoporous Mater. 296 (2020) 110015, https://doi.org/10.1016/j.micromeso.2020.110015.

[21] A. Marcilla, M. Beltran, A. Gómez-Siurana, I. Martinez, D. Berenguer, Template removal in MCM-41 type materials by solvent extraction. Influence of the treatment on the textural properties of the material and the effect on its behaviour as catalyst for reducing tobacco smoking toxicity, Chem. Eng. Res. Des. 89 (2011) 2330–2343, https://doi.org/10.1016/j.cherd.2011.04.015.

[22] S. Kawi, M.W. Lai, Supercritical fluid extraction of surfactant template from MCM-41, Chem. Commun. (1998) 1407–1408, https://doi.org/10.1039/a802907e.

[23] I. Melián-Cabrera, F. Kapteijn, J.A. Moulijn, Room temperature detemplation of zeolites through H2O 2-mediated oxidation, Chem. Commun. 1 (2005) 2744–2746, https://doi.org/10.1039/b502167g.

[24] J. Kecht, T. Bein, Oxidative removal of template molecules and organic functionalities in mesoporous silica nanoparticles by H2O2 treatment, Microporous Mesoporous Mater. 116 (2008) 123–130, https://doi.org/10.1016/j.micromeso.2008.03.027.

[25] H. Xing, Y. Zhang, M. Jia, S. Wu, H. Wang, J. Guan, L. Xu, T. Wu, Q. Kan, Detemplation with H2O2 and characterization of MCM-56, Catal. Commun. 9 (2008) 234–238, https://doi.org/10.1016/j.catcom.2007.06.006.

[26] Y. Hu, Y. Zhang, Y. Tang, Rapid detemplation of nanozeolite β: microwave-assisted Fenton-like oxidation, RSC Adv. 2 (2012) 6036–6041, https://doi.org/10.1039/c2ra00947a.

[27] J. Kuhn, J. Gascon, J. Gross, F. Kapteijn, Detemplation of DDR type zeolites by ozonication, Microporous Mesoporous Mater. 120 (2009) 12–18, https://doi.org/10.1016/j.micromeso.2008.09.018.

[28] J. Kuhn, M. Motegh, J. Gross, F. Kapteijn, Detemplation of [B]MFI zeolite crystals by ozonication, Microporous Mesoporous Mater. 120 (2009) 35–38, https://doi.org/10.1016/j.micromeso.2008.08.061.

[29] A.H. Khoja, A. Mazhar, F. Saleem, M.T. Mehran, S.R. Naqvi, M. Anwar, S. Shakir, N.A. Saidina Amin, M.B. Sajid, Recent developments in catalyst synthesis using DBD plasma for reforming applications, Int. J. Hydrogen Energy 46 (2021) 15367–15388, https://doi.org/10.1016/j.ijhydene.2021.02.043.

[30] C.W. Jones, K. Tsuji, T. Takewaki, L.W. Beck, M.E. Davis, Tailoring molecular sieve properties during SDA removal via solvent extraction, Microporous Mesoporous Mater. 48 (2001) 57–64, https://doi.org/10.1016/S1387-1811(01)00330-4.
[31] L.M. Parker, D.M. Bibby, J.E. Patterson, Thermal decomposition of ZSM—5 and silicalite precursors, Zeolites 4 (1984) 168–174, https://doi.org/10.1016/0144-2449(84)90056-3.
[32] C.-Y. Chen, S.L. Burkett, H.-X. Li, M.E. Davis, Studies on mesoporous materials II. Synthesis mechanism of MCM-41, Microporous Mater. 2 (1993) 27–34, https://doi.org/10.1016/0927-6513(93)80059-4.
[33] L. Lang, S. Zhao, J. Jiang, W. Yang, X. Yin, Importance of hydrogen for low-temperature detemplation of high-silica MFI zeolite crystals, Microporous Mesoporous Mater. 235 (2016) 143–150, https://doi.org/10.1016/j.micromeso.2016.07.044.
[34] J.Y. Lai, F. Twaiq, L.H. Ngu, Recycling of surfactant template in mesoporous MCM-41 synthesis, IOP Conf. Ser. Mater. Sci. Eng. 206 (2017), 012044, https://doi.org/10.1088/1757-899X/206/1/012044.
[35] Hyunjoo Lee, I. Stacey, Zones, Mark E. Davis, A combustion-free methodology for synthesizing zeolites and zeolite-like materials, Nature 425 (2003) 383–385, https://doi.org/10.1038/nature01988.1.
[36] J. Ryczkowski, J. Goworek, W. Gac, S. Pasieczna, T. Borowiecki, Temperature removal of templating agent from MCM-41 silica materials, Thermochim. Acta 434 (2005) 2–8, https://doi.org/10.1016/j.tca.2004.12.020.
[37] J.S. Beck, J.C. Vartuli, W.J. Roth, M.E. Leonowicz, C.T. Kresge, K.D. Schmitt, C.T. W. Chu, D.H. Olson, E.W. Sheppard, S.B. McCullen, J.B. Higgins, J.L. Schlenker, A new family of mesoporous molecular sieves prepared with liquid crystal templates, J. Am. Chem. Soc. 114 (1992) 10834–10843, https://doi.org/10.1021/ja00053a020.
[38] R. Schmidt, D. Akporiayea, M. Stöcker, O.H. Ellestad, Synthesis of Al-containing MCM-41 materials: template interaction and removal, Stud. Surf. Sci. Catal. 84 (1994) 61–68, https://doi.org/10.1016/S0167-2991(08)64097-5.
[39] A. Corma, V. Fornes, M.T. Navarro, J. Perezpariente, Acidity and stability of MCM-41 crystalline aluminosilicates, J. Catal. 148 (1994) 569–574, https://doi.org/10.1006/jcat.1994.1243.
[40] J.M. Kim, J.H. Kwak, S. Jun, R. Ryoo, Ion exchange and thermal stability of MCM-41, J. Phys. Chem. 99 (1995) 16742–16747, https://doi.org/10.1021/j100045a039.
[41] A. Montes, E. Cosenza, G. Giannetto, E. Urquieta, R.A. De Melo, N.S. Gnep, M. Guisnet, Thermal decomposition of surfactant occluded in mesoporous MCM-41 type solids, Stud. Surf. Sci. Catal. 117 (1998) 237–242, https://doi.org/10.1016/s0167-2991(98)80997-x.
[42] M.T.J. Keene, R.D.M. Gougeon, R. Denoyel, R.K. Harris, J. Rouquerol, P. L. Llewellyn, Calcination of the MCM-41 mesophase: mechanism of surfactant thermal degradation and evolution of the porosity, J. Mater. Chem. 9 (1999) 2843–2849, https://doi.org/10.1039/a904937a.
[43] F. Kleitz, W. Schmidt, F. Schüth, Evolution of mesoporous materials during the calcination process: structural and chemical behavior, Microporous Mesoporous Mater. (2001) 44–45, https://doi.org/10.1016/S1387-1811(01)00173-1, 95–109.
[44] F. Kleitz, W. Schmidt, F. Schüth, Calcination behavior of different surfactant-templated mesostructured silica materials, Microporous Mesoporous Mater. 65 (2003) 1–29, https://doi.org/10.1016/S1387-1811(03)00506-7.
[45] V. Meynen, P. Cool, E.F. Vansant, Verified syntheses of mesoporous materials, Microporous Mesoporous Mater. 125 (2009) 170–223, https://doi.org/10.1016/j.micromeso.2009.03.046.
[46] N. Chaouati, A. Soualah, M. Chater, M. Tarighi, L. Pinard, Mechanisms of coke growth on mordenite zeolite, J. Catal. 344 (2016) 354–364, https://doi.org/10.1016/j.jcat.2016.10.011.
[47] B.P. Feuston, J.B. Higgins, Model structures for MCM-41 materials: a molecular dynamics simulation, J. Phys. Chem. 98 (1994) 4459–4462, https://doi.org/10.1021/j100067a037.
[48] K. Deekamwong, J. Wittayakun, Template removal by ion-exchange extraction from siliceous MCM-41 synthesized by microwave-assisted hydrothermal method, Microporous Mesoporous Mater. 239 (2017) 54–59, https://doi.org/10.1016/j.micromeso.2016.09.049.
[49] V. Kanazirev, G.L. Price, The effect of O2on the thermal activation of zeolite beta, J. Catal. 161 (1996) 156–163, https://doi.org/10.1006/jcat.1996.0172.
[50] E.M. Gallego, C. Paris, M.R. Díaz-Rey, M.E. Martínez-Armero, J. Martínez-Triguero, C. Martínez, M. Moliner, A. Corma, Simple organic structure directing agents for synthesizing nanocrystalline zeolites, Chem. Sci. 8 (2017) 8138–8149, https://doi.org/10.1039/c7sc02858j.
[51] A. Astafan, M.A. Benghalem, Y. Pouilloux, J. Patarin, N. Bats, C. Bouchy, T.J. Daou, L. Pinard, Particular properties of the coke formed on nano-sponge *bEA zeolite during ethanol-to-hydrocarbons transformation, J. Catal. 336 (2016) 1–10, https://doi.org/10.1016/j.jcat.2016.01.002.